

Distributed feedback lasing based on a negative-index metamaterial waveguide

BRYCE A. TENNANT,^{1,*} RIFFAT ARA,² ABDULAZIZ ATWIRI,² GOVIND P. AGRAWAL,³ NATALIA M. LITCHINITSER,⁴ AND DREW N. MAYWAR^{1,2}

¹Microsystems Engineering, Rochester Institute of Technology, Rochester, New York 14623, USA

²Electrical, Computer, and Telecommunications Engineering Technology, Rochester Institute of Technology, Rochester, New York 14623, USA

³The Institute of Optics, University of Rochester, Rochester, New York 14627, USA

⁴Department of Electrical and Computer Engineering, Duke University, Durham, North Carolina 27708, USA

*Corresponding author: bat3289@rit.edu

Received 10 June 2019; accepted 9 August 2019; posted 19 August 2019 (Doc. ID 369057); published 13 September 2019

This Letter lays the foundation of a new type of distributed feedback (DFB) laser whose optical feedback is due to the evanescent coupling between an active positive-index material (PIM) waveguide and a lossy negative-index metamaterial (NIM) waveguide. Active PIM–NIM coupled-mode equations are presented and solved to characterize the dispersion relation, resonant optical gain, and lasing. The photonic bandgap of this grating-less DFB laser does not depend on a Bragg wavenumber, but depends on the difference between the wavenumbers of the PIM and NIM waveguides; controlling this wavenumber difference allows for single-mode lasing and, ultimately, single-mode broadband lasing. © 2019 Optical Society of America

<https://doi.org/10.1364/OL.44.004586>

Distributed feedback (DFB) lasers are commonly found in high-performance communication systems requiring thermal stability, narrow linewidth, and moderately high optical power. DFB in commercial lasers is accomplished by forming a first-order diffraction grating in the real part of the refractive index. This traditional kind of DFB produces two lowest-threshold longitudinal lasing modes, one on either side of the photonic bandgap [1]. To realize a single-mode laser, this degeneracy is commonly broken by fabrication steps such as shifting the grating phase in the center of the structure by $\pi/2$ (i.e., a $\lambda/4$ shift) [2], or by optimizing the reflectivity of each end facet [3].

A new method for achieving DFB has been recently proposed and modeled based on the evanescent coupling of a positive-index material (PIM) waveguide to a negative-index metamaterial (NIM) waveguide [4–6]. Metamaterials offer remarkable electrodynamic behavior stemming from a negative refractive index [7]; despite having a negative refractive index, a NIM sandwiched between PIM has been predicted to support the propagation of a transverse optical mode [8–10]. Notably, the Poynting vector of an optical field traveling through a NIM waveguide can have the opposite direction as the associated wave vector [6,8]. Such a NIM waveguide, when evanescently

coupled to a PIM waveguide, creates a distributed coupling region where power flows in either longitudinal direction [4].

Coupled-mode equations for the PIM–NIM structure were first presented for passive, lossless waveguides and revealed a reflectivity spectrum characteristic of DFB [4]. Coupled-mode equations were then extended to the case of a nonlinear lossless PIM–NIM structure and used to study optical bistability [5]. These studies were performed for passive structures.

In this Letter, we leverage PIM–NIM DFB to form a new kind of DFB laser. Specifically, we consider an active PIM–NIM structure in which the gain is provided by the PIM waveguide over the length of the coupling region L , as shown in Fig. 1. To study this active structure, we extend the PIM–NIM coupled-mode equations to include gain for the PIM waveguide and loss for the NIM waveguide. This model predicts the occurrence of lasing with unique dependencies on waveguide parameters not found in traditional active DFB structures.

The electric-field amplitudes in the PIM and NIM waveguides are given by $E_A(z) = A(z)e^{-i\Delta\beta z}$ and $E_B(z) = B(z)e^{i\Delta\beta z}$, respectively, where A and B are the slowly varying complex-field amplitudes of a relative rotating frame,

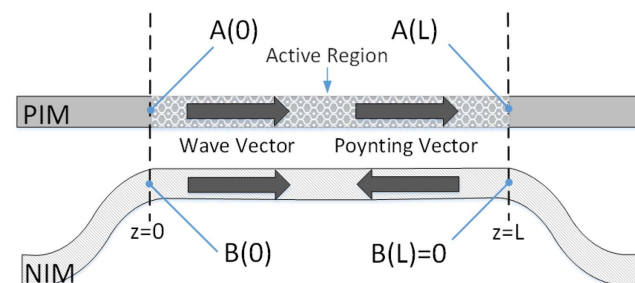


Fig. 1. Schematic of a PIM–NIM DFB laser, where the active region of a PIM waveguide is evanescently coupled to a lossy NIM waveguide over length L . The (white) cladding regions surrounding the waveguides are PIM. The counter-directional nature of the Poynting vectors in either waveguide results in distributed feedback, resonant optical gain, and, ultimately, lasing.

$\Delta\beta = (\beta_A - \beta_B)/2$ is the detuning parameter, and β_A and β_B are the corresponding modal wavenumbers. The coupled-mode equations for optical-field amplitudes A and B within the PIM–NIM structure are posited as

$$\frac{dA}{dz} = \left(i\Delta\beta + \frac{g}{2} \right) A + i\kappa_{np}B, \quad (1a)$$

$$-\frac{dB}{dz} = \left(i\Delta\beta - \frac{\alpha}{2} \right) B + i\kappa_{pn}A, \quad (1b)$$

where g is the net gain coefficient of the PIM, α is the loss coefficient of the NIM, and κ_{pn} and κ_{np} are the coupling coefficients for coupling into the NIM and PIM, respectively. We have assumed that the anisotropy of each waveguide is small, a common assumption for coupled-mode equations and for previous modeling work in PIM–NIM couplers [4–6].

These coupled-mode equations are similar in form to those of a traditional DFB laser, whose counter-propagating A and B field amplitudes traverse a *single* waveguide and are coupled via a diffraction grating [1,11]. One significant difference is that for the traditional DFB laser, the detuning parameter $\Delta\beta = \beta_0 - \beta_\Lambda$, where β_0 is the wavenumber of both optical modes, $\beta_\Lambda = \pi/\Lambda$ is the Bragg wavenumber, and Λ is the period of the diffraction grating. Also, since the counter-propagating modes traverse the *same* active waveguide, they each experience the gain coefficient g [i.e., $\alpha \rightarrow -g$ in Eq. (1b)]. For the PIM–NIM structure, the exclusive appearance of g or α in either equation results in important sum and difference expressions that govern the resonant amplification and lasing behavior.

The eigenvalues of the coupled-mode equations describe the behavior of the PIM–NIM structure and are solved for as

$$q_+ = \frac{\delta}{4} + i\sqrt{\left(\Delta\beta - i\frac{\sigma}{4} \right)^2 - \kappa^2}, \quad (2a)$$

$$q_- = \frac{\delta}{4} - i\sqrt{\left(\Delta\beta - i\frac{\sigma}{4} \right)^2 - \kappa^2}, \quad (2b)$$

where

$$\kappa = \sqrt{\kappa_{pn}\kappa_{np}}, \quad \sigma = g - \alpha, \quad \delta = g + \alpha. \quad (3)$$

The quantity σ is the *round-trip* gain coefficient for light that propagates down the full length of the PIM waveguide followed by a return trip down the full length of the NIM waveguide (without evanescent coupling throughout). The quantity δ is the disparity from transparency and equals zero only for passive, lossless waveguides. Compared to the eigenvalues of a traditional DFB laser [11], $\sigma/2$ takes the place of the traditional DFB gain coefficient, while the δ term is entirely new.

The imaginary portion of either eigenvalue q directly reveals the photonic bandgap nature of the active PIM–NIM structure, as illustrated in Fig. 2 for several values of the round-trip gain σ normalized by κ . For $\sigma = 0$, a photonic bandgap occurs between $\Delta\beta = \pm\kappa$, wherein optical fields exponentially decay in the direction of the Poynting vector. Increasing σ produces oscillatory, decaying optical fields within the photonic bandgap, as is the case for the traditional DFB laser [1]. For the

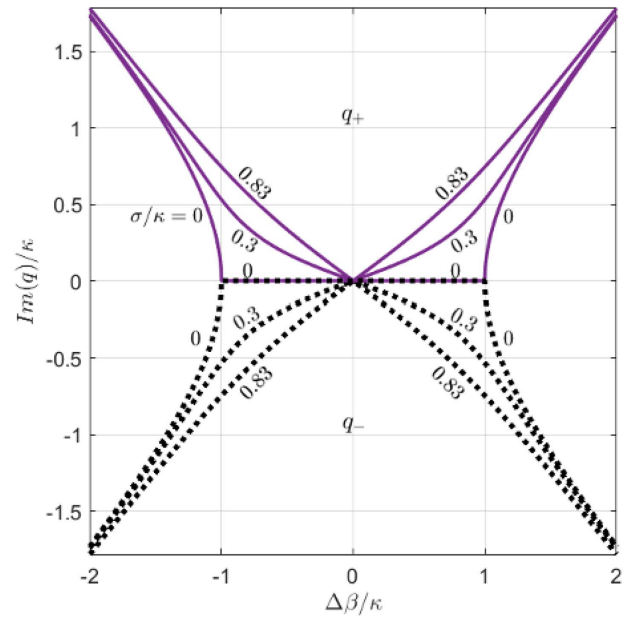


Fig. 2. Dispersion relations for the q_+ eigenvalue (upper half-plane) and q_- eigenvalue (lower half-plane) for $\sigma/\kappa = 0, 0.3$, and $2.5/3$. A photonic bandgap is clearly seen for $\sigma = 0$, and the disparity quantity δ does not impact the dispersion relations.

PIM–NIM structure, the dispersion relations are independent of the disparity quantity δ .

The eigenvalues given by Eqs. (2a) and (2b) form the following general solutions of the amplitudes A and B :

$$A(\zeta) = A_1 e^{q_+ L \zeta} + A_2 e^{q_- L \zeta}, \quad (4a)$$

$$B(\zeta) = B_1 e^{q_+ L \zeta} + B_2 e^{q_- L \zeta}, \quad (4b)$$

where $\zeta = z/L$ is the normalized longitudinal spatial coordinate, and A_1, A_2, B_1 , and B_2 are constant coefficients.

Amplification of optical power between the ends of the PIM waveguide is studied by disallowing an optical signal in the NIM waveguide at $z = L$; i.e., $B(\zeta = 1) = 0$. Applying this boundary condition after substituting the eigenvalue Eqs. (2a) and (2b) into the amplitude Eqs. (4a) and (4b) yields

$$A(\zeta) = -\frac{2B_1 e^{(\delta L/4)\zeta}}{e^{-ibL\kappa_{pn}L}} [\psi L \sinh(ibL(\zeta - 1)) + bL \cosh(ibL(\zeta - 1))], \quad (5a)$$

$$B(\zeta) = \frac{2B_1 e^{(\delta L/4)\zeta}}{e^{-ibL}} \sinh(ibL(\zeta - 1)), \quad (5b)$$

where the following quantities do not depend on the disparity δ :

$$b = \sqrt{\psi^2 - \kappa^2}, \quad \psi = \Delta\beta - i\frac{\sigma}{4}. \quad (6)$$

The field amplitudes at the ends of the PIM–NIM structure are determined by a substitution of the appropriate value of ζ :

$$A(\zeta = 0) = \frac{2B_1}{e^{-ibL}\kappa_{pn}L} [\psi L \sinh(ibL) - bL \cosh(ibL)], \quad (7a)$$

$$A(\zeta = 1) = -\frac{2B_1 e^{\delta L/4} bL}{e^{-ibL}\kappa_{pn}L}, \quad (7b)$$

$$B(\zeta = 0) = -\frac{2B_1}{e^{-ibL}} \sinh(ibL). \quad (7c)$$

The transmittivity T and reflectivity R expressions are found from the ratio of field amplitudes as follows:

$$t = \frac{A(\zeta = 1)}{A(\zeta = 0)} = \frac{-e^{(\delta L/4)} bL}{\psi L \sinh(ibL) - bL \cosh(ibL)}, \quad (8a)$$

$$r = \frac{B(\zeta = 0)}{A(\zeta = 0)} = \frac{-\kappa_{pn}L \sinh(ibL)}{\psi L \sinh(ibL) - bL \cosh(ibL)}, \quad (8b)$$

$$T = |t|^2 = \frac{e^{(\delta L/2)} |bL|^2}{|\psi L \sinh(ibL) - bL \cosh(ibL)|^2}, \quad (9a)$$

$$R = |r|^2 = \frac{|\kappa_{pn}L|^2 |\sinh(ibL)|^2}{|\psi L \sinh(ibL) - bL \cosh(ibL)|^2}. \quad (9b)$$

The transmittivity T of an active PIM–NIM structure is shown in Fig. 3(a) for $\kappa L = 3$ and a NIM-waveguide loss $\mathcal{L} = 5$ dB, where $\mathcal{L} = \exp(-\alpha L)$. Resonant amplification is exhibited on either side of the photonic bandgap. The resonances increase in strength as the value of the PIM-waveguide gain $G = \exp(gL)$ is increased, and their peak transmittivity exceeds 30 dB for $G = 15$ dB. For detuning $\Delta\beta L$ away from the photonic bandgap, the dissimilarity in modal wavenumbers prevents efficient coupling between waveguides; this inefficiency results in a transmittivity T that is equivalent to the gain of the uncoupled PIM waveguide G .

Lasing is achieved when the transmittivity peak T_p reaches infinity, physically corresponding to obtaining an optical output power without an optical input power [11]. The increase in T_p as a function of the normalized PIM gain coefficient gL is shown in Fig. 3(b) for $\kappa L = 3$ and several values of NIM loss \mathcal{L} . T_p is seen to increase at a low rate for small gL and eventually rises in an extreme manner as gL approaches the lasing-threshold value $g_{th}L$. The threshold $g_{th}L$ increases as the NIM loss \mathcal{L} increases.

The relation between lasing-threshold values across different NIM-loss cases is seen clearly when the peak transmittivity T_p is considered in terms of the round-trip gain σL . As shown in Fig. 3(c), the value of $\sigma_{th}L$ is the *same* regardless of the amount of the NIM loss \mathcal{L} . Since the disparity $\delta = \sigma + 2\alpha$ [from Eqs. (3)], each curve in Fig. 3(c) corresponds to a unique value of δL , and therefore the lasing threshold $\sigma_{th}L$ is independent of δL .

The threshold and detuning of lasing modes for DFB resonators can be obtained by deeper consideration of the transmittivity expression [1]. Equation (9a) for T becomes infinite when its denominator becomes zero, which happens in the non-trivial case when

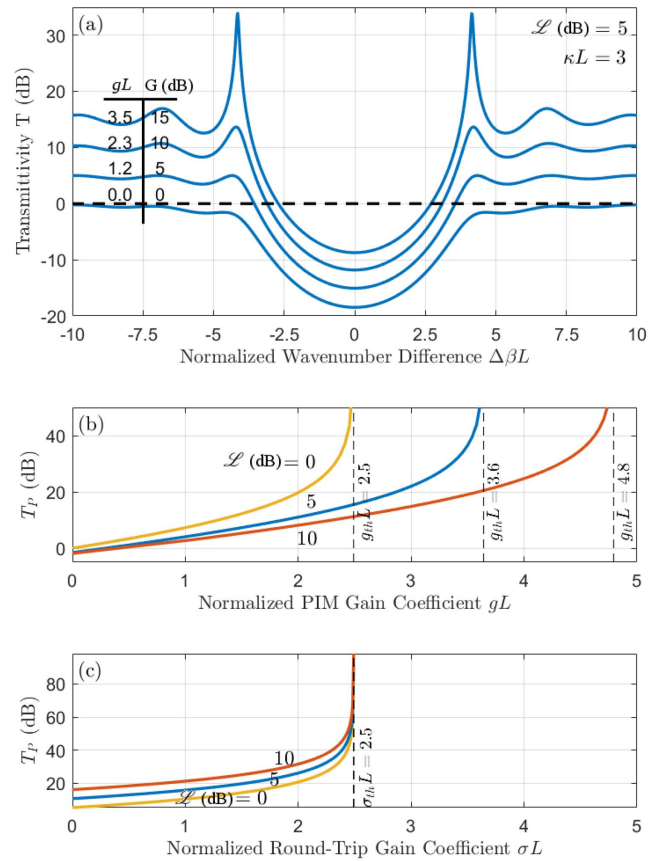


Fig. 3. Resonant optical-amplification route to lasing threshold. (a) The transmittivity spectrum for a NIM loss of 5 dB reveals resonant optical amplification at the edges of the photonic bandgap. Increasing the PIM gain increases the strength of the resonances. Transmittivity far from $\Delta\beta L = 0$ is at the level of an uncoupled, active PIM. (b) Peak transmittivity T_p as a function of PIM gain coefficient gL for three values of NIM loss \mathcal{L} . Lasing threshold $g_{th}L$ occurs when $T_p = \infty$ and depends on the NIM loss. (c) T_p as a function of normalized round-trip gain σL ; lasing threshold $\sigma_{th}L$ is independent of the NIM loss \mathcal{L} and disparity δ . $\kappa L = 3$ for all subfigures.

$$\psi_{th}L \sinh(ib_{th}L) = b_{th}L \cosh(ib_{th}L), \quad (10)$$

where the subscripts explicitly indicate that the quantities ψ and b are at their lasing-threshold values. Expanding the square of Eq. (10), applying Eq. (6), and applying the identity $\cosh^2 x - \sinh^2 x = 1$ yields, after some manipulation,

$$\frac{\sigma_{th}L}{4} + i\Delta\beta_{th}L = \pm i\kappa L \cosh(ib_{th}L). \quad (11)$$

Substitution of Eq. (11) back into Eq. (10) ultimately generates the following transcendental equation relating $b_{th}L$ to the normalized coupling coefficient κL :

$$\kappa L = \pm \frac{b_{th}L}{\sinh(ib_{th}L)}. \quad (12)$$

The solution pairs $\{\kappa L, b_{th}L\}$ are found from Eq. (12) by a numerical solver. These solution pairs are then fed into the right-hand side of Eq. (11), and the real and imaginary parts are used to determine $\sigma_{th}L$ and $\Delta\beta_{th}L$. This approach to

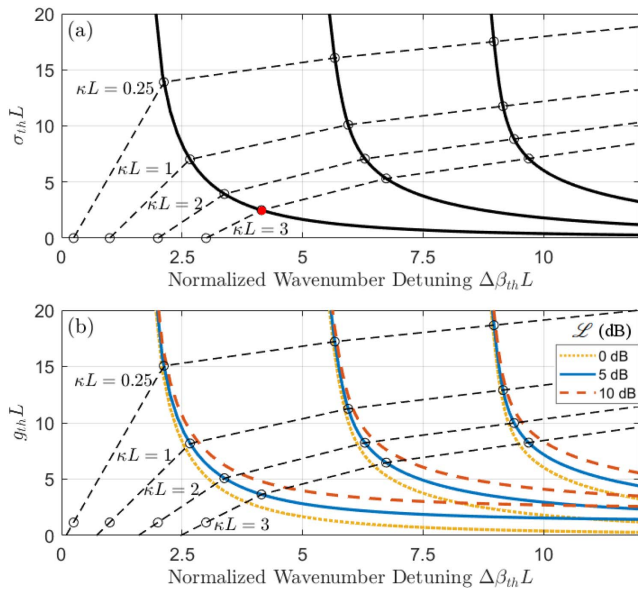


Fig. 4. Lasing-mode spectrum as a function of coupling κL using transcendental Eqs. (11) and (12); the three lowest lasing-threshold modes are shown for positive $\Delta\beta_{th}L$ (symmetric modes for negative $\Delta\beta_{th}L$ not shown). (a) Lasing threshold $\sigma_{th}L$ and wavenumber detuning $\Delta\beta_{th}L$ solution pairs for specific coupling-coefficient values, several of which are highlighted using dashed lines. The red solid dot indicates the solution found in Fig. 3(c). (b) Lasing threshold expressed as $g_{th}L$ and for three values of NIM loss \mathcal{L} , where $\mathcal{L} = 5$ dB has been used for the κL highlight lines.

studying lasing also shows that the lasing threshold $\sigma_{th}L$ is independent of the NIM loss \mathcal{L} and disparity δ .

The threshold values $\sigma_{th}L$ and $\Delta\beta_{th}L$ of the three lowest lasing-threshold modes are shown in Fig. 4(a), where only the curves for positive $\Delta\beta_{th}L$ are shown (a symmetric set occurs for negative $\Delta\beta_{th}L$). Each point on a mode curve is associated with a specific value of the normalized coupling coefficient κL , and constant-coupling examples across the mode spectra are indicated using dashed lines. The red solid marker in the figure represents the lasing threshold that limits the amplification behavior shown in Fig. 3(a). The impact of the NIM loss \mathcal{L} can be made explicit by applying $g_{th} = \sigma_{th} + \alpha$ [from Eqs. (3)] to the data in Fig. 4(a). Doing so yields the threshold $g_{th}L$ and $\Delta\beta_{th}L$ pairs shown in Fig. 4(b); each lasing mode is now represented by multiple curves, one for each value of NIM loss.

Although the lasing-threshold curves shown in Fig. 4 are similar in form to those of the traditional DFB laser [1], a significant difference in the behavior of either kind of DFB laser is rooted in the definition of $\Delta\beta_{th}L$. For a traditional DFB laser, $\Delta\beta = \beta - \frac{\pi}{\Lambda}$, and so the center of the photonic bandgap ($\Delta\beta L = 0$) is achieved when the free-space wavelength λ matches the Bragg wavelength $\lambda_B = 2n\Lambda$, where n is the modal index. Since the photonic bandgap spans only up to a couple of nanometers, the lowest lasing-threshold mode on either side of the photonic bandgap experiences similar gain, leading to the undesirable dual-lasing-mode nature of these devices [1–3].

For a PIM–NIM DFB laser, $\Delta\beta \propto \beta_A - \beta_B$, and so the center of the photonic bandgap ($\Delta\beta L = 0$) is achieved only if the modal wavenumbers β_A and β_B are equal; equivalently, since $\beta_A - \beta_B = \frac{2\pi}{\lambda}(n_A - n_B)$, the center of the photonic bandgap is achieved only if the modal indices n_A and n_B are equal. Matching the wavenumbers to yield $\Delta\beta L = 0$ is commonly achieved in traditional directional couplers (DCs) made of two PIM waveguides [12]. For the PIM–NIM DFB laser, it may be possible to design the waveguides so that the wavenumbers *never* match over the gain spectrum. Doing so would force $\Delta\beta L$ to be solely positive or negative, thereby breaking the lasing-threshold mode degeneracy and giving rise to a single-mode laser.

Another intriguing prospect for the PIM–NIM DFB laser is the possibility to design the wavenumbers to have a *constant* difference $\Delta\beta L = C$ over a broad wavelength spectrum. Traditional DCs (made of two PIM waveguides) use this approach to achieve broadband wavelength operation by designing $\Delta\beta L = C = 0$ [13]. In the case of a PIM–NIM DFB laser, designing $\Delta\beta L = C = \Delta\beta_{th}L$ over a broad wavelength spectrum would allow for single-mode lasing over a broad wavelength spectrum, i.e., a solution point for a lasing mode in Fig. 4(a), such as the red solid dot, would span a broad range of wavelengths. Additional investigation is required to study the behavior of this broadband single-mode laser and how it differs from the traditional broadband laser based on multiple longitudinal modes.

This Letter presents a new type of DFB laser, one based on the evanescent coupling between an active PIM waveguide and a lossy NIM waveguide. Since the lasing behavior depends on the difference between modal wavenumbers, its behavior is not restricted by a grating-defined Bragg wavenumber; controlling the wavenumber difference allows for single-mode lasing and, ultimately, single-mode broadband lasing.

REFERENCES

1. H. Kogelnik and C. Shank, *J. Appl. Phys.* **43**, 2327 (1972).
2. H. Haus and C. Shank, *IEEE J. Quantum Electron.* **12**, 532 (1976).
3. T. Matsuoka, Y. Yoshikuni, and G. Motosugi, *Electron. Lett.* **21**, 1151 (1985).
4. A. Alu and N. Engheta, in *Negative-Refraction Metamaterials: Fundamental Principles and Applications*, G. V. Eleftheriades and K. G. Balmain, eds. (Wiley, 2005), Chap. 9, pp. 339–375.
5. N. M. Litchinitser, I. R. Gabitov, and A. I. Maimistov, *Phys. Rev. Lett.* **99**, 113902 (2007).
6. W. Yan, L. Shen, Y. Yuan, and T. J. Yang, *J. Lightwave Technol.* **26**, 3560 (2008).
7. V. G. Veselago, *Sov. Phys. Uspekhi* **10**, 509 (1968).
8. I. V. Shadrivov, A. A. Sukhorukov, and Y. S. Kivshar, *Phys. Rev. E* **67**, 057602 (2003).
9. T. Amemiya, S. Yamasaki, M. Tanaka, H. Kagami, K. Masuda, N. Nishiyama, and S. Arai, *Opt. Express* **27**, 15007 (2019).
10. T. Amemiya, T. Kanazawa, S. Yamasaki, and S. Arai, *Materials* **10**, 1037 (2017).
11. D. N. Maywar and G. P. Agrawal, *IEEE J. Quantum Electron.* **33**, 2029 (1997).
12. D. L. Lee, *Electromagnetic Principles of Integrated Optics* (Wiley, 1986).
13. Y. Wang, Z. Lu, M. Ma, H. Yun, F. Zhang, N. A. Jaeger, and L. Chrostowski, *IEEE Photon. J.* **8**, 1 (2016).